Inhibition of Non-Homologous End-Joining for DNA Repair: A Modeling Approach

Andrew Alamban, Steven Fried, & Jericho Lawson
The University of Arizona
Mentor: J. Rubin Abrams
MATH 485: Mathematical Modeling, Spring 2020

ABSTRACT. DNA damage from radiation sources poses critical challenges to cell survival and is often harnessed in radiotherapy towards the destruction of cancer tumors. Hence, elucidating cellular repair mechanisms to damaged DNA is a key step towards understanding and enhancing radiotherapy. We analyze a proposed mathematical model describing the method of non-homologous end-joining (NHEJ) for repair of double-stranded DNA breaks induced by ionizing radiation. The model accounts for enzyme-mediated and mass action kinetics of steps involved in NHEJ, producing a system of coupled ordinary differential equations whose behavior is simulated using a stiff-ODE solver in MATLAB. Initial work has verified the model's applicability toward measuring DSB repair kinetics against experimental data for DSB repair kinetics in cell lines. Moreover, we demonstrate applications of the model toward investigating inhibition of enzymes involved in NHEJ, with the given examples of DNA-dependent protein kinase (DNA-PK) and a Ligase-IV containing catalytic complex (abbreviated XXL). Competitive or noncompetitivie inhibitors of these enzymes, including Wortmannin and the Ligase-IV inhibitor Compound 189, prove to be most effective at restricting DSB-repair in tumor cells within our simulations. Further research will aim to more accurately place NHEJ in the context of total DSB repair and tie the DSB-repair model to cancer cell mortality, offering significant new tools in the development of radiotherapy-coupled chemotherapies.

Key Words: DNA repair, Double-stranded break (DSB), Non-homologous end-joining (NHEJ), Mathematical modeling, Radiotherapy, Ionizing radiation (IR).

1. Introduction & Background

Information for life is encoded in polymers called deoxyribonucleic acid (DNA). Proper maintenance and replication of DNA allow for its propagation into the next generation, while dysfunction can lead to generally debilitating effects such as cell death and mutation. A number of sources may be responsible for DNA damage, including chemical reactivity and electromagnetic radiation of varying linear energy transfers (LETs). Each of these sources can lead to varying forms of damage, ranging from adduct formation and base excision for some types of chemical damage, pyrimidine dimerization in the case of lower-energy ultraviolet radiation damage, and double-stranded breaks (DSBs) in the DNA in the case of higher-LET ionizing radiation (IR) [6].

Due to the debilitating effects of DNA damage to cell function and survival, cells have developed a number of ways of repairing damage. Understanding these DNA repair pathways are a key front in cancer biology, where DNA damage can be both an instigator of cancer (through improper repair leading to mutation), and an advantageous means of eradicating cancer cells such as through radiotherapy. Numerous research over the last century has hence sought to understand diverse mechanisms of DNA damage and repair.

The 1930s-1940s gave rise to early studies on the deleterious effects of ultraviolet and ionizing radiation (IR) on organisms, and cellular responses to these effects. This time period witnessed the discovery of the photoreactivation pathway for the repair of thymine dimers, the very first known

DNA-repair mechanism [6]. Following Watson and Crick's structural characterization of the DNA double helix in 1953, the DNA-repair field advanced lightyears by introducing new biochemical sophistication to studying and clarifying DNA repair mechanisms. New mechanisms discovered in the 1960s and 1970s included base-excision repair (BER) and double-stranded break (DSB) repair, the latter of which is a key cellular strategy toward combating programmed cell death or genomic instability [6].

In order to carry out DSB repair, organisms have fortunately evolved mechanisms of DSB repair including homologous recombination (HR) and microhomology-mediated end joining (MMEJ) [20]. Of interest, however, is non-homologous end-joining (NHEJ), as it is the most prominent DSB repair mechanism in humans, which reconnects the broken ends of DNA independent of a homologous template [4]. Studies on NHEJ have yielded a mechanistic description regarding the proteins responsible for DSB repair [12]. Of interest in the mechanism are two enzymes. One of these, DNA-PKcs, is responsible for the signaling that processes complex DSBs into simpler DSBs. Ultimately, DSBs are then ligated together by the second target of interest, the XXL complex which is a protein complex composed of XLF, XRCC4, and the ligase IV complex [17]. These two players in NHEJ can be inhibited by Wortmannin [11] and Compound 189 [2]. However, a mathematical model for inhibitor effect on DSB repair dynamics is currently unknown. By reviewing current mathematical models of DNA repair [17; 13; 3], we reiterated a specific NHEJ model, which involves monitoring the dynamics of 11 species involved in NHEJ [17]. We then modified the model to incorporate the effects of enzyme inhibition, considering different types of inhibition and different concentration doses for each inhibitor.

2. Literature Review

The field of radiation biology has long been interested in how organisms, particularly single cells, respond to radiation-induced DNA damage. An outcome of interest to most researchers is the relationship between surviving cells and the dose of radiation inflicted. The linear-quadratic model, which contains the empirically determined parameters α and β, has been used to model cell survival S as a function of radiation dose D [13]:

$$S = e^{-\alpha D - \beta D^2} \tag{2.1}$$

Due to growing information regarding genetic makeup of species as well as molecular pathways regarding DNA repair, the linear-quadratic model has become outdated because it employs parameter sets that do not translate well to pathological cases, such as cancer.

McMahon, *et al.*, propose a new model giving rise to a parameter set that can be fitted using experimental data constants. This provides robust parameters that lead to a high correlation between simulated and experimental data. Previous models often use different parameter sets for a specific cellular response (e.g. number of DSB, mutation rates, cell survival, etc.) but the proposed model allows prediction for different cellular response using one parameter set. In addition, this parameter set can be applied across different cell lines and different conditions [13].

Double-stranded break (DSB) repair depends on the distance between the free ends; i.e., the further two ends are from each other, the more difficult it will be for them to rejoin. Similarly, the fidelity of DSB repair also depends on which mechanism the cell employs. Their model considers three repair pathways: 1) non-homologous end joining (NHEJ) 2) homologous recombination (HR) and 3) microhomology-mediated end joining (MMEJ). Each pathway has its own respective repair rate as well as repair fidelity. Depending on the genetics, some pathways may also vary in

use or, in some cases, not be usable because of mutation. Lastly, the complexity of the DSB also depends on the linear energy transfer (LET) of the radiation [13].

McMahon, *et al.* constructed their parameter set consisting of a characteristic repair distance, pathway-dependent repair rate, and fidelity, the probability of a complex DSB-repair given geometric considerations that are cell-dependent. They then produced analytical solutions of exponential decay to model the dynamics of DSB repair as well as create probabilistic models to account for the use of different repair pathways. Each of these models correlated well with experimental data, including the observations of repair kinetics, DSB misrepair, mutation rate, chromosomal aberrations (which differ from DSB misrepair in terms of scope), and cell survival [13].

The benefits of McMahon's model is that its application is bidirectional. On the input side, one can fit experimental data with a simulated curve from the model. This will give information that the experiment did not investigate. For example, the authors cite how kinetics of H2AX, a DSB-response protein, and aberration data can inform how DSB repair processes fail. On the output side, one can obtain mutation or survival response predictions using fitted parameters from other experiments [13].

In conclusion, McMahon *et al.* have presented a model which allows for the prediction of various cellular outcomes from a single set of parameters that can be applied to different cell types under various conditions [13]. The authors, however, commented that most of their assumptions were done on the scale of in vitro experiments. Additionally, their model did not take advantage of molecular mechanisms to radiation response. By incorporating well-studied molecular mechanisms, one can come up with a more granular model which will be desirable in treating tumors, as tumors are genetically heterogeneous.

Such an approach was proposed in 2018 by Rouhani, who modeled DSB repair by NHEJ. Several known empirical qualities of NHEJ are used in the construction of a biochemical mechanism that is kinetically modeled by a system of 11 coupled, ordinary differential equations. These models make use of either standard mass-action kinetics (in the case of binding/dissociation reactions) or Michaelis-Menten kinetics (in the case of enzymatic reactions), to model the interconversions between 11 different species appearing in the biochemical pathway. Parameters for these reactions (14 in total) were gathered from sources reported in the literature [17].

In Rouhani's model, the bifurcation of DSB repair, occurring by either a fast or a slow mechanism, is explained by the formation of ligatable (85%) and unligatable (15%) complexes from the broken DNA and recruited Ku proteins. Ligatable complexes may be immediately rejoined by an enzymatic XXL complex composed of ligase IV, XRCC4, and XLF proteins. Unligatable complexes, on the other hand, must first bind DNA-dependent protein kinase catalytic subunits (DNA-PKcs), and be rejoined into a ligatable complex by a hyperphosphorylated Artemis enzyme, whose phosphorylation levels are controlled by both the DNA-PKcs–DSB complexes and ATM enzyme. The ligatable complex is then rejoined enzymatically by an XXL complex, as in the fast mechanism. Generally, the fast and slow mechanisms are delegated to simple and more complex DSBs, respectively [17].

The system of stiff ordinary differential equations mechanistically modeling NHEJ was simulated using the ode15s solver in MATLAB and compared against experimentally measured kinetics of DSB repair in various cell lines. These include normal, ATM-deficient, and Artemis-deficient cell lines (both human fibroblast and mouse embryonic), subjected to varying dosages of ionizing radiation between 0.02 and 2 Gy. Prior to the publication of this paper, it was unknown whether the ligatable complexes of DSB with Ku produced in the fast reaction mechanism could still bind DNA-PKcs or not. By evaluating two different models, one allowing this step and one not, and

comparing simulation results to experimental data, it was determined that the inclusion of this step significantly increases model accuracy. The model including this DNA-PKcs binding step demonstrated P-values above 0.72 for all radiation levels and correlation coefficients above 0.97 for the normal human cells and above 0.88 for the normal mouse cells. ATM-deficient human cells demonstrated a strong correspondence to the model, with P-values above 0.75 and correlation coefficients above 0.93 for all radiation levels tested, while Artemis-deficient human cells corresponded to the model with P-values and correlation coefficients more than 0.87 and 0.95, respectively [17].

In summary, Rouhani's theorized biochemical pathway describing DSB repair by NHEJ results in a mathematical model that is highly accurate at predicting the kinetics of DSB repair in experimental systems. The model results indicate that the most important parameters controlling NHEJ rate are the Ku protein initial concentration, followed by XXL complex initial concentration and enzymatic activity, and then DNA-PKcs initial concentration and Artemis initial concentration and enzymatic activity. By prioritizing the pharmacological inhibition of NHEJ directors in this order, one takes a closer step towards effectively hindering this process in cancer cells subjected to radiotherapy, thereby increasing the success rate in radiotherapeutic treatment of cancer patients [17].

In addition to DSB repair, alternate types of DNA damage and their repair mechanisms have been explored and analyzed mathematically. For instance, a model for the formation of DNA adducts from oxidative estrogen metabolism and base-excision repair (BER) of the adducts was proposed by Crooke and Parl (2010) in their paper "A Mathematical Model for DNA Damage and Repair." The model is separated into two different stages: 1) the formation of adducts leading to apurinic (AP) sites (i.e. single-nucleotide DNA damage) and 2) the repair of these adducts using BER.

In the first stage of the model, mass action kinetics were used where the estrogen quinone forms adducts spontaneously without any enzyme involvement [3]. Michaelis-Menten kinetics were then used to model enzymatic reactions. Crooke and Parl also found direct experimental evidence that oxidative metabolism of hormone E_2 leads to the formation of deoxyribonucleoside adducts [3].

The second stage of the model is based on the BER pathway. BER is modeled by a system of nonlinear differential equations, once again invoking Michaelis-Menten kinetics. All k constants found in the system are based on experimental values. After testing these models, Crooke and Parl found several key factors governing damage and repair. It was noted, for instance, that doubling the concentration of E_2 doubles the number of AP sites, or empty places along a DNA strand with no nucleotide [3]. Additionally, it was shown that commonly occurring variants of CYP1B1 differ in activity of producing $4-OHE_2$ from the parent hormone. Not only that, but the more active CYP1B1 variant increased DNA damage [3].

Ultimately, Crooke and Parl's model shows dynamic interaction between the estrogen-mediated DNA damage and the DNA base-excision repair pathway in order to show the overall impact on carcinogenesis on DNA. The model predicts a larger increase in the number of AP sites, which indicates the involvement of other factors including enzymatic factors.

In total, approaches in mathematically modelling a range of DNA repair mechanisms have been reported. McMahon, *et. al* have proposed a model for DSB repair that incorporated three repair pathways, leading to simulations that can predict different outcomes in addition DSB repair [13]. Rouhani proposed a mechanistic model specifically for NHEJ which accurately predicts DSB repair dynamics and expands upon the role that DNA-PKcs plays in NHEJ [17]. Lastly, Crooke and Parl's mechanistic model of DNA adduct formation was compared with experimental data and their BER repair model incorporated parameters derived from experimental data [3].

Together, the literature show significant progress in simulating DNA repair. While McMahon, *et al.* created a model that can account for different repair pathways, their model failed to account for the mechanistic pathways reported in literature. Integration of mechanistic models such as one proposed by Rouhani would increase the prediction power of generalized models of NHEJ. To take a step further, integration of other types of DNA damage and repair, as discussed by Crooke and Parl, would describe a more realistic scenario as organisms are constantly exposed to more than one type of DNA damage. Formulation of more accurate models could be used to further basic science as well as improve applications of radiotherapy in healthcare.

3. Replication of Rouhani's Results

3.1. Summary of Model

The model presented by Rouhani showcases the process of non-homologous end joining [17]. Figure 3.1 visualizes that very step-by-step process. As mentioned earlier, the slow and fast phases of the DSB repair are included in this model.

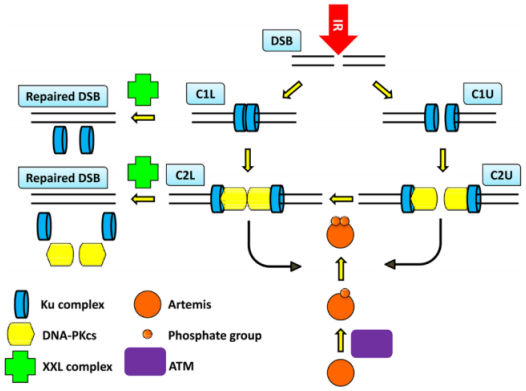

FIGURE 3.1. NHEJ Model [17]

Rouhani discovered that the model can be composed of a system of 11 ODEs, each with very specific components. To better organize the ODEs, nine dummy variables were used. Appendix A highlights those choices.

Each of these nine dummy variables represents a certain part of the diagram in Figure 3.1. v_1 represents the use of IR dosage to develop double strand breaks. v_2 represents the chemical reaction of the double strand breaks and two sets of the Ku complexes to form C1L and C1U. v_3 and v_4 each represent chemical reactions of one ligatable or unligatable C1 complex and two molecules of DNA-PKcs to form the ligatable or unligatible C2 complex respectively [17]. The rest of the dummy variables are a result of reaction rates that can be described by the Michaelis-Menten equation, which can be represented as the following:

$$r = \frac{k_{cat}[\mathrm{E}][\mathrm{S}]}{K_{\mathrm{M}} + [\mathrm{S}]}, \tag{3.1}$$

where r is the reaction rate, $[E]$ and $[S]$ are the enzyme and substrate concentrations, k_{cat} is the maximum rate of product formation, and K_m is the substrate concentration in which the reaction rate reaches half of the maximum rate. As such, v_5 is equivalent to the use of C1L complexes to produce repaired double strand breaks and two Ku complexes. Likewise, v_6 involves the use of

C2L complexes to repair double strand breaks and produce two Ku complexes and two DNA-PKcs proteins. v_7 involves the usage of ArtemisPP to convert C2U complexes to C2L complexes. v_8 represents the use of ATM to convert Artemis to phosphorylated Artemis. Likewise, v_9 encapsulates the transformation of phosphorylated Artemis to hyperphosphorylated Artemis using DNA-PKcs proteins [17].

With these dummy variables in place to simplify the ongoing processes in the model, we can now write the system of 11 ODEs as the following:

$$\begin{aligned}
\frac{d[DSB]}{dt} &= v_1 - v_2 \\
\frac{d[Ku]}{dt} &= -2v_2 + 2v_5 + 2v_6 \\
\frac{d[C1L]}{dt} &= 0.85v_2 - v_3 - v_5 \\
\frac{d[C1U]}{dt} &= 0.15v_2 - v_4 \\
\frac{d[DNA-PKcs]}{dt} &= -2v_3 - 2v_4 + 2v_6 \\
\frac{d[C2L]}{dt} &= v_3 - v_6 + v_7 \\
\frac{d[C2U]}{dt} &= v_4 - v_7 \\
\frac{d[Repaired\,DSB]}{dt} &= v_5 + v_6 \\
\frac{d[Artemis]}{dt} &= -v_8 \\
\frac{d[ArtemisP]}{dt} &= v_8 - v_9 \\
\frac{d[ArtemisPP]}{dt} &= v_9
\end{aligned} \tag{3.2}$$

Terms that are either in blue or green will be discussed in the next subsection.

3.2. Approach & Results

Our first objective is to replicate the results that were found in Rouhani's paper, particularly the model that is proposed. Within MATLAB, there is a script called ODE15s, which is described as a stiff differential equation solver. Considering the complexity of the model, using a script like this is crucial to our replication status. For this model, we will use the initial concentrations that Rouhani used in her model and if stated, we will use the model 1 versions of the concentrations (e.g. $K_m\,ArtemisPP = 240$).

A MATLAB script with two various functions is used. The first function includes all dummy v variables and the 11 ODES that will need to be solved using the ODE15s functionality; the second function computes the result of Michealis-Menten equations, given the enzyme and substrate concentrations, the maximum rate of product formation, and the substrate concentration at half the

maximum rate. The main MATLAB script contains several initial conditions, the ODE15s function call, and any plots. For any initial concentrations aside from the initial number of double strand breaks and the ones mentioned in Rouhani's paper, we set these values to zero. In our model, we set the initial number of double strand breaks to $c \times IRdose$ and used a time span from 0 to 100 hours, similar to what is seen in Rouhani's work.

Figures 2-5 from Rouhani's paper were replicated. Our first replication involves comparing two different models for the proposed NHEJ schematic mentioned by Rouhani. Figure 3.2 shows the remaining double strand breaks over time following radiation for models 1 and 2 [17]. To find the amount of remaining double strand breaks at time t, we took the amount of repaired double strand breaks at time t and subtracted the amount from the initial amount of DSBs (i.e. when $t = 0$). Both graphs have negative exponential behavior similar to those in Rouhani's research. Additionally, all values relatively match the values that Rouhani had in her paper when there is an IR dosage of 2 grays of X-rays. While there is strong replication of the models, there were slight modifications that were made to match the graphs in Rouhani's paper. Primarily, the $\frac{d[DSB]}{dt}$ term had to be changed to just $-v_2$. Additionally, terms associated with dummy variable v_3 were removed from the system of ODEs for model 2. This is the result of the step associated with v_3, which involves the conversion of the C1L complex to the C2L complex, not taking place in model 2. This removal differentiates model 1 from model 2. Aside from those modifications, the replication itself was a huge success for this diagram.

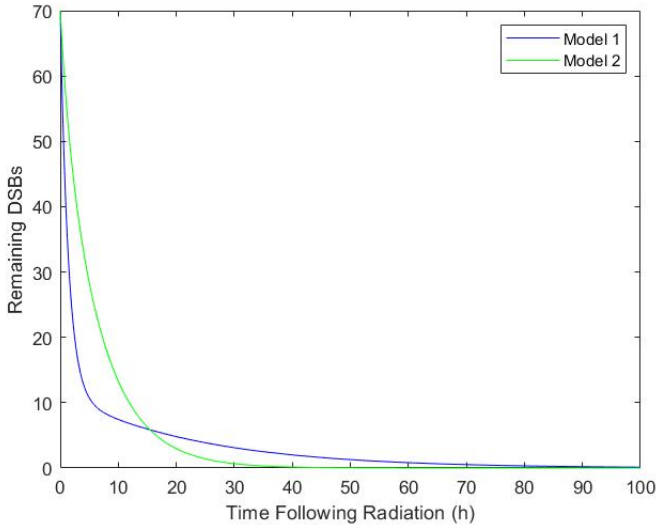

FIGURE 3.2. Replicated results of models 1 and 2 from Rouhani's paper using 2 Gy X-rays.

Other figures from Rouhani's were also replicated to verify the paper's significance. These figures plot remaining double-stranded breaks over time based on modifications to either concentrations of IR dosage or the ATM enzyme in the system. Appendices B-D show the various replications of these plots. In Appendix B, different plots are made considering the different IR dosages that are used to induce initial double-stranded breaks. 0.02, 0.2, 1.3, and 2.0 Grays of IR dosage are tested to see how the rate of the repair of double-stranded breaks changes. Successful replication of these figures occurred. Most of the repair occurs during the first five hours in all plots, showing how quick DNA repair can relatively occur. In Appendix C, the figures represent

how the rate of DNA repair changes with either one or zero ATM enzyme(s). The first graph in Appendix C shows the rate of DNA repair with no ATM in the system. Replication of this figure proved to be a success. Notice that the repair of double-stranded breaks flattens out at around 11 as time goes to infinity. This is due to the lack of ATM that would be needed to process the slow pathway; without any ATM, the pathway cannot continue with any DNA repair. The other figures in Appendix C show how the effects of various doses of ionizing radiation and 1 ATM enzyme affect the process of DNA repair. Lower amounts of ionizing radiation do smooth out the graph over time. Nonetheless, the replication of these figures were also successful. In Appendix D, analysis is done to see how the lack of Artemis affects DNA repair. This time, 140 ATM enzymes are used at 2 and 1.3 Grays of ionizing radiation. Again, the curve flattens out at around 15% of the initial concentration of double-stranded breaks due to the importance of Artemis in the slow pathway. Additionally, these figures are successfully replicated.

In all, replication of the models from Rouhani's paper is a success. However, reproduction of the experimental data seen in those figures were not done. The successful reproduction of Rouhani's simulated data may be tested by using statistical tests to compare the mathematical model to experimental data. Rouhani reports a variety of experimental data describing DSB repair kinetics due to NHEJ in both human and mouse fibroblast embryonic cell lines [17]. These data include cellular responses to varying radiation doses (0.02 Gy, 0.2 Gy, 1.3 Gy, and 2 Gy) for wild-type, Artemis-deficient, and ATM-deficient cell lines. As a future direction, we propose to recreate the conditions simulating each of these conditions using the described model, and to compare the simulated curves to reported experimental data by calculating coefficients of determination R^2 and regression p-values, the latter of which can be calculated using polynomial terms to account for curvature. With the successful replication of the models, we look to extend Rouhani's models by including enzyme inhibition into the models.

4. Enzyme Inhibition Modeling in NHEJ

4.1. Modeling Enzyme Inhibition: Methods

Having verified the accuracy of our model, we next investigate medical applications of our model, specifically toward radiotherapy. The principle of radiotherapy hinges upon the destruction of cancer cells through targeted damage to cancer cell DNA by ionizing radiation (IR). Cancer cells, in response, will attempt to repair damaged DNA or undergo apoptosis. Hindering the repair of IR-induced DSBs is thus advantageous in promoting cancer cell death. The model proposed herein suggests that several proteins and enzymes involved in the NHEJ mechanism could be chemically targeted for inhibition in conjunction with radiotherapy, making the radiotherapy more potent against cancer. Specifically, reduction of available Ku proteins and inhibition of the enzymatic XXL complex are expected to have the greatest effect on NHEJ inhibition, since these proteins are universally involved in NHEJ no matter the specific pathway taken (fast or slow). The enzymatic activities of DNA-PKcs and Artemis should matter to a lesser extent, as these proteins are only involved in select routes of the NHEJ pathway.

Enzyme inhibition can occur by varying mechanisms that are classified by the type of complex the inhibitor binds. Competitive inhibitors bind the free enzyme, precluding some enzyme from binding substrate; uncompetitive inhibitors bind enzyme-substrate complexes to preclude the release of reacted substrate as product. Also possible are mixed inhibitors, which bind both free enzyme and enzyme-substrate complexes. We shall consider each type of inhibition by their impacts on Michaelis-Menten enzyme parameters. Competitive inhibitors increase the value of K_{M}

to decrease substrate binding affinity as follows, [I] represents inhibitor concentration and K_{I}, the dissociation constant of the enzyme to its inhibitor:

$$K_{\mathrm{M}}^{+\mathrm{I}} = K_{\mathrm{M}}(1 + \frac{[\mathrm{I}]}{K_{\mathrm{I}}}). \tag{4.1}$$

Uncompetitive inhibitors reduce both k_{cat} and K_{M} by the same constant value:

$$K_{\mathrm{M}}^{+\mathrm{I}} = \frac{K_{\mathrm{M}}}{(1 + \frac{[\mathrm{I}]}{K_{\mathrm{I}}})} \tag{4.2}$$

and

$$k_{\mathrm{cat}}^{+\mathrm{I}} = \frac{k_{\mathrm{cat}}}{(1 + \frac{[\mathrm{I}]}{K_{\mathrm{I}}})}. \tag{4.3}$$

One common type of mixed inhibitor is the noncompetitive inhibitor, which binds to free enzyme and enzyme-substrate complex with equal affinity to the effect of decreasing the parameter k_{cat} according to equation 4.3 without altering K_{I}. Hence, using this process we simulate the impact of real and hypothetical inhibitors to these enzymes by scaling the parameters appropriately and evaluating the impact on the NHEJ timescale. Note that in order to perform these calculations, we must convert between molar concentrations of inhibitors and molecules per cell values for the enzymes, which is accomplished using an average human fibroblast cell volume of 2000 cubic microns.

4.2. Modeling Enzyme Inhibition: Comparison of Inhibition Modes

We first consider hypothetical cases of inhibition for both DNA-PK and the XXL complex, which are perhaps the best characterized in terms of inhibition. Few inhibitors of Artemis are known at present, with little quantitative data existing for those thought to be inhibitors [14]. In the case of DNA-PK, however, we consider hypothetical competitive, uncompetitive, and noncompetitive inhibitors with $K_{\mathrm{I}} = 6.0\ \mu$M, reminiscent of the known DNA-PK inhibitor LY294002 [11]. Likewise, in the case of the XXL complex, we consider hypothetical competitive, uncompetitive, and noncompetitive inhibitors with $K_{\mathrm{I}} = 5.0\ \mu$M, reminiscent of the known ligase IV inhibitor Compound 189. By administering equal concentrations of each inhibitor type to a particular enzyme, the resulting trends reveal important distinctions between the different inhibition trends (Figure 4.1).

We observe that competitive and noncompetitive inhibition are highly indistinguishable from one another, where their respective curves of DSB-repair kinetics appear superimposed on one another in the above figure. Likewise, the case of uncompetitive inhibition is not significantly different from the case of no inhibition, and these curves also appear superimposed with the exception of some slight deviation early in the post-radiation phase for the XXL complex. The reasons for these observations become abundantly clear as we consider the Michaelis-Menten kinetics of both enzymes. We note that the value of the Michaelis-Menten constant K_{M} for each enzyme is approximately three orders of magnitude greater than the DSB-substrate concentration in the cell following 2 grays ionizing radiation, indicating a far greater concentration of free enzyme than enzyme-substrate complex. Hence, we reach a limiting behavior of the Michaelis-Menten equation (3.1) where the concentration of the substrate in the denominator is negligible. Letting

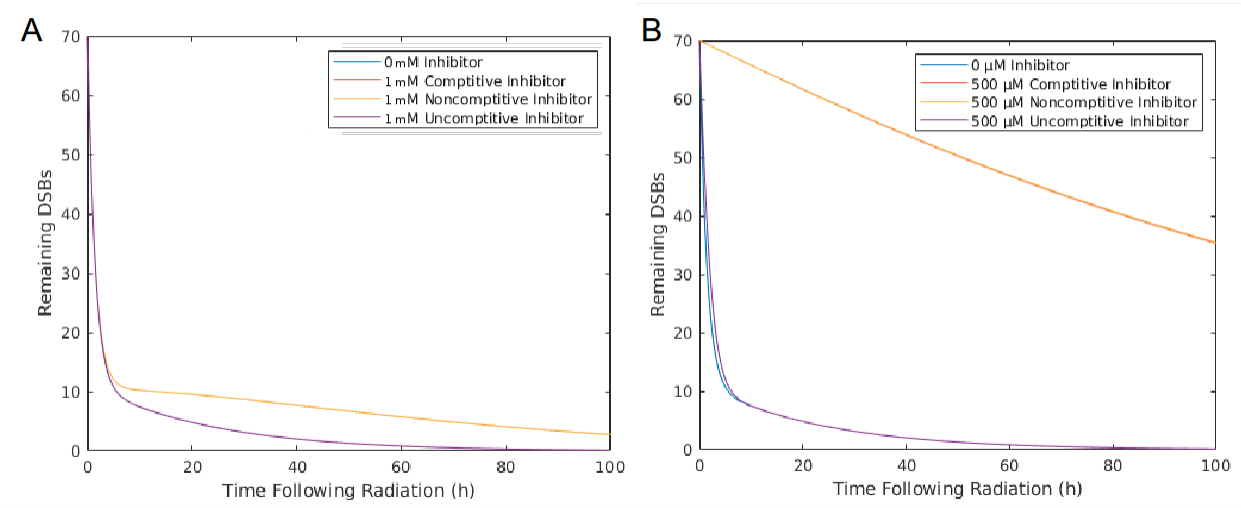

FIGURE 4.1. Theoretical effects of three inhibition modes are simulated based on their interactions with DNA-Pk (A) and the XXL complex (B).

$\alpha = (1 + \frac{I}{K_I})$, then for competitive inhibition,

$$r = \frac{k_{cat}[\mathrm{E}][\mathrm{S}]}{\alpha K_\mathrm{M} + [\mathrm{S}]}. \tag{4.4}$$

Note that for low substrate concentration [S] this equation is virtually indistinguishable from that for noncompetitive inhibition:

$$r = \frac{\frac{k_{cat}}{\alpha}[\mathrm{E}][\mathrm{S}]}{K_\mathrm{M} + [\mathrm{S}]}. \tag{4.5}$$

Likewise, the rate equation for uncompetitive inhibition is virtually indistinguishable from that for no inhibition at all (3.1) at low substrate concentrations, since the inhibitor effects on K_M nullify those of k_cat:

$$r = \frac{\frac{k_{cat}}{\alpha}[\mathrm{E}][\mathrm{S}]}{\frac{K_\mathrm{M}}{\alpha} + [\mathrm{S}]}. \tag{4.6}$$

We therefore conclude that an effective inhibitor of either DNA-PK or the XXL complex must have the capability to bind to the free-enzyme, generating either competitive or noncompetitive inhibition. Specifically, inhibitors with high affinity for the free enzyme are expected to have the greatest result in slowing DSB-repair kinetics in irradiated cancer cells.

4.3. Modeling Enzyme Inhibition: Simulations of Known Inhibitors

Fortunately, some known cases of competitive or noncompetitive inhibitors have been verified thus far in the quest to increase radiation-induced cancer cell mortality. We explore five potential inhibitors to DNA-PK: the noncompetitive inhibitor Wortmannin, and the competitive inhibitors LY294002, Rutin, Quercetin, and Quercitrin. These inhibitors have experimentally verified K_I values of 120 nM, 6.0 μM, 26 μM, 110 μM, and 208 μM, respectively [11]. Likewise, we consider

the inhibition of ligase IV in the XXL enzymatic complex. One known inhibitor, discovered as Compound 189 by Chen *et al.*, is a known competitive inhibitor of ligase IV with $K_I = 5\mu$M [2].

In the case of DNA-PK inhibitors, we consider the case of equal concentrations (1 mM) for each of the five experimentally verified inhibitors, and simulate the resulting alterations to DSB-repair kinetics (Figure 4.2):

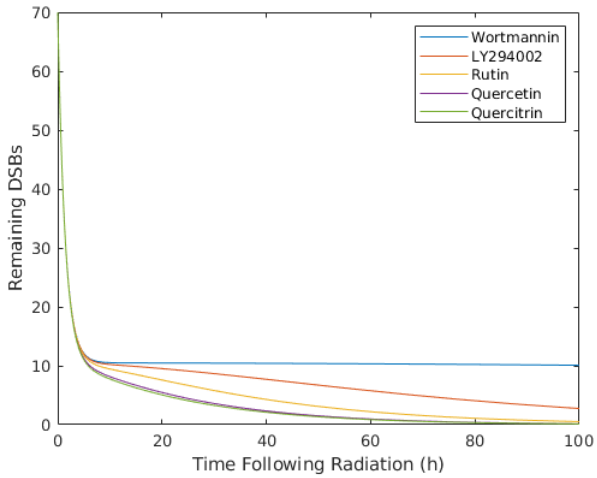

FIGURE 4.2. Simulated DSB-repair kinetics in the presence of equal concentrations (1mM each) of five known inhibitors of DNA-PK.

The simulated results indicate the most significant alteration to DSB-repair kinetics in the case of Wortmannin. This is predictable given that Wortmannin has the greatest binding-affinity of any of the inhibitors to DNA-PK, with K_I = 120 nM. It is also notable, however, that the inhibitor LY294002 similarly leads to a nonzero number of DSBs remaining after 100 hours. We can moreover simulate the titration of varying concentrations of Wortmannin into the cell to observe the concentration dependence of this inhibitor (Figure 4.3):

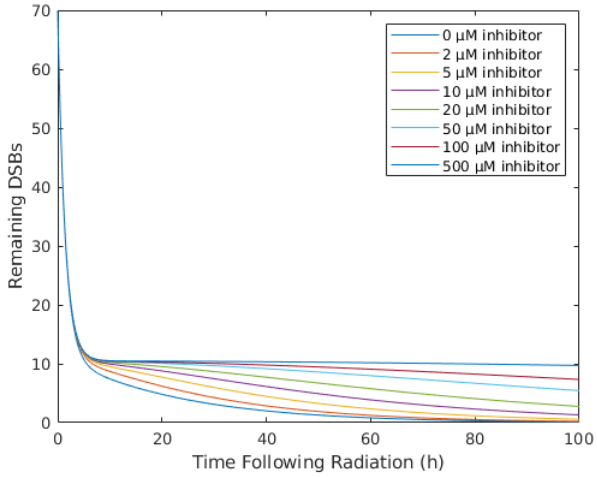

FIGURE 4.3. Simulated DSB-repair kinetics in the presence of varying concentrations of Wortmannin.

The change in DSB-repair kinetics with increasing Wortmannin concentration is intriguingly characterized by a change in long-term behavior, but not initial rate, of DSB repair. While the initial repair rate is approximately constant no matter the inhibitor concentration, the long-term repair rate changes significantly with the addition of Wortmannin, approaching a limiting behavior of approximately 15% of DSBs remaining. This behavior is highly indicative of the role of DNA-PK in processing complex breaks, occurring approximately 10-20% of the time in response to high linear-energy-transfer radiation. Because DNA-PK is not involved in processing simple breaks, the fast pathway of NHEJ goes unhindered and the initial repair rate corresponding to the resolution of these simple breaks goes unchanged. However, because the long-term repair rate is highly dependent on DNA-PK in processing complex breaks, Wortmannin can play a significant role in slowing this process, with the limiting case where processing of complex breaks is completely halted and 15% of DSBs remain unrepaired.

In a similar vein, we model the alterations to DSB-repair kinetics in the presence of Compound 189, a $K_{\mathrm{I}} = 5\mu$M inhibitor of the enzyme Ligase IV within the XXL complex (Figure 4.4).

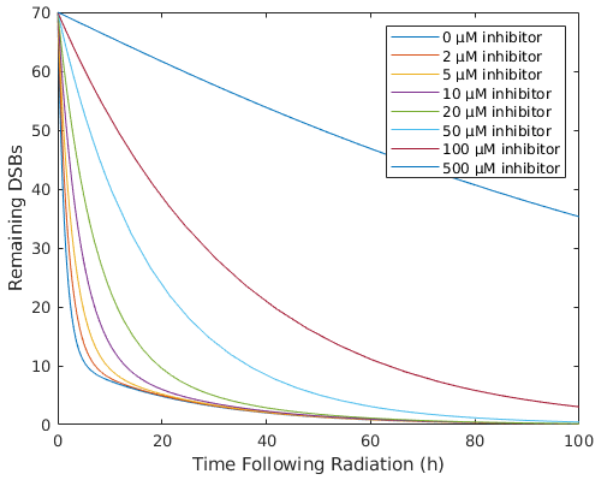

FIGURE 4.4. Simulated DSB-repair kinetics in the presence of varying concentrations of Compound-189, a Ligase IV inhibitor.

In drastic contrast to Wortmannin, Compound 189 significantly affects the initial DSB-repair rate, in addition to the long-term rate of repair. This is attributed to the fact that the XXL complex is involved in processing both simple and complex breaks, thus not distinguishing between the slow and the fast NHEJ pathways. In the short term, then, Compound 189 has a much more significant effect on slowing DSB repair compared to Wortmannin. Given Wortmannin's higher affinity for its respective enzyme DNA-PK, however, the long-term effects of a low concentration of Wortmannin will be more substantial than the long-term effets of a low concentration of Compound 189.

4.4. Modeling Enzyme Inhibition: Optimization of Inhibitor Concentrations

For the purposes of dosage optimization, we consider the number of DSBs remaining after 100 hours in the presence of varying concentrations of either Wortmannin or Compound 189. While this may not necessarily translate directly to certain cancer cell death, as this is a more complex relationship requiring more detailed modeling to consider, the remaining DSBs after 100 hours presents a useful metric for comparing relative long-term effectiveness of various inhibitors. In

Figure 4.5, the remaining DSBs after 100 hours are plotted as a function of varying concentrations of either Wortmannin or Compound 189 as a comparison of effectiveness.

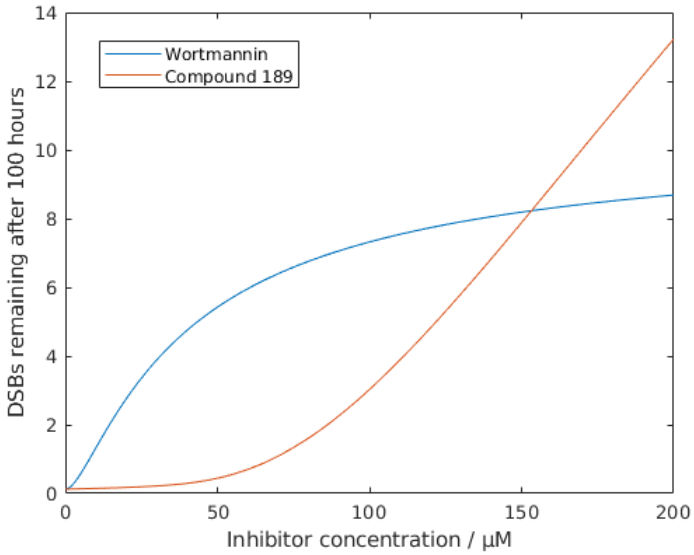

FIGURE 4.5. Simulated number of double-stranded breaks remaining after 100 hours for varying concentrations of Wortmannin or Compound 189.

The results show unequivocally that Wortmannin is a more appropriate inhibitor in low concentrations (below 150 μM), while Compound 189 is more effective at leading to more DSBs remaining after 100 hours for high inhibitor concentrations (above 150 μM). It is also possible to perform an optimization of the first derivatives of these trends, finding the inflection points of remaining DSBs as a function of inhibitor concentration. For Wortmannin, this inflection point occurs at 10 μM, while for Compound 189, this occurs at 170 μM. These concentrations demonstrate a point of "diminishing returns", above which the differential increase in DSBs remaining after 100 hours is not as great as this increase is below the critical concentration.

Given the effectiveness of Compound 189 at inhibiting the fast kinetics of DSB repair, and of Wortmannin at inhibiting slow kinetics of DSB repair, we predict that a combination of both drugs, assuming human tolerance of either in the appropriate concentrations requested, will be most effective toward enhancing radiotherapy against cancer cells. For instance, in Figure 4.6, an effective inhibition of NHEJ in the presence of both inhibitors at concentrations indicative of their respective 100-hour inflection points is demonstrated. After 100 hours, at least 10 double-stranded breaks still exist in the cell, which is anticipated to drastically increase cancer cell mortality. The exact magnitude of the rate of cancer cell apoptosis is highly dependent on a number of factors including cancer cell type and rate of division, which entail significant opportunities for future research.

5. Future Plans & Discussion

5.1. Alternate Proposed NHEJ Mechanisms

Some controversy exists yet in the literature on the role of hyperphosphorylation of Artemis in NHEJ [15][8]. We hence propose to investigate additional situations where singly phosphorylated

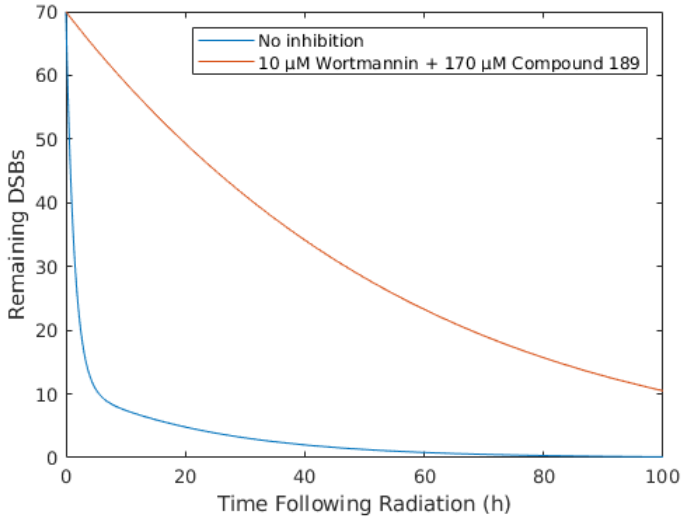

FIGURE 4.6. Simulated DSB-repair kinetics in the case of uninhibited cells, and cells with concentrations of Wortmannin and Compound 189 at their respective inflection points for remaining DSBs after 100 hours.

Artemis, or even unphosphorylated Artemis, perform the same catalytic ligation step in the NHEJ mechanism. As an initial alternate scenario, we plan to investigate the case where ArtemisP and ArtemisPP have the same catalytic activity, which is simply adressed by changing the form of equation

$$v_7 = \frac{k_{cat}ArtemisPP \times ([ArtemisPP] + [ArtemisP]) \times 2 \times [C2U]}{K_m ArtemisPP + 2 \times [C2U]}. \tag{5.1}$$

Likewise, we can consider a case where all forms of Artemis, phosphorylated or not, have the same enzymatic activity:

$$v_7 = \frac{k_{cat}ArtemisPP \times ([ArtemisPP] + [ArtemisP] + [Artemis]) \times 2 \times [C2U]}{K_m ArtemisPP + 2 \times [C2U]}. \tag{5.2}$$

As a more sophisticated method of addressing the role of Artemis phosphorylation in NHEJ, we may consider Artemis, ArtemisP, and ArtemisPP has three different enzymes, each with their own Michaelis-Menten parameters:

$$\begin{aligned} v_7 = &\frac{k_{cat}ArtemisPP \times ([ArtemisPP]]) \times 2 \times [C2U]}{K_m ArtemisPP + 2 \times [C2U]} + \frac{k_{cat}ArtemisP \times ([ArtemisP]]) \times 2 \times [C2U]}{K_m ArtemisP + 2 \times [C2U]} \\ &+ \frac{k_{cat}Artemis \times ([Artemis]]) \times 2 \times [C2U]}{K_m Artemis + 2 \times [C2U]}. \end{aligned} \tag{5.3}$$

Significantly, this model introduces four new parameters. In the event that experimental values for these parameters cannot be determined, we may consider a range of hypothetical values as a means of estimating the impact of these alternate situations on NHEJ kinetics. Specifically, we hypothesize successively smaller values of k_{cat} and/or larger values of K_M for decreasing phosphorylation levels, highlighting an enzymatic activity that is phosphorylation-dependent, yet more complex than a simple on-off switch.

5.2. NHEJ in the Broader Context of DSB Repair

It is important to recall that NHEJ is not the sole method of DSB repair in the cell. Additional means include homologous recombination (HR) and microhomology-mediated end-joining, which are typically slower and employed for more complex breaks that involve damage to nucleotides in the vicinity of the DSB, or multiple breaks on each strand [19]. To this end, McMahon *et al.* has proposed a simplified kinetic model describing all three methods of DSB repair together as a linear combination of exponential functions:

$$N(t) = N_0(p_f e^{-\lambda_f t} + p_s e^{-\lambda_s t} + p_m e^{-\lambda_m t}), \tag{5.4}$$

where $N(t)$ is the total number of DSBs after a time t, N_0 is the initial DSB number, λ_x are the three repair rate constants (NHEJ - **f**ast, HR - **s**low, and **m**icrohomology, respectively), and p_x is the probability of a break being repaired by each process [13]. While advantageous in that the macroscopic model accounts for each of the three repair processes, the model falls short in its accuracy of how each molecular process is individually modeled. For instance, the NHEJ model is more complex than an exponential function, and a next-level more accurate DSB repair model will thus incorporate the NHEJ model of Rouhani into the linear combination of exponentials proposed by McMahon *et al.*. Since the Rouhani model is described by a system of ordinary differential equations rather than an algebraic function, its behavior may be computationally simplified by fitting a smoothing spline to the simulation in MATLAB and incorporating this spline into the McMahon *et al.* linear combination of exponentials.

In addition to NHEJ, we propose to consider existing mathematical models of homologous recombination (HR) and microhomology-mediated end-joining (MMEJ), such as the coupled ODE-system for MMEJ proposed by Taleei and Nikjoo for DSB-repair in the G1 and early S phase of the cell cycle [20]. Successful simulation of one or more of these alternative pathways to DSB repair will enable incorporation into the combined McMahon model, giving information on the synergistic cooperation between three different DSB repair methods.

5.3. Broader Effects of DNA-PKcs Inhibition by Wortmannin

While Wortmannin is well-studied, Compound 189 has only been used in original research for a few times [2; 9]. Our model of enzyme inhibition and its effects on DSB repair kinetics is motivated by the accuracy of Rouhani's model of NHEJ that simulates the dynamics of γ-H2AX phosphorylation - a marker of DSBs [16]- in mammalian fibroblast cell lines [17]. To our knowledge, however, measurement of DSB dynamics using the γ-H2AX assay in the presence of Wortmannin has only been done in DNA-PKcs-deficient SCID cells [10]. The obtained parameters for the K_m and k_{cat} herein were obtained from *in vitro* experiments. To confirm the validity of our modified NHEJ model via Wortmannin-mediated DNA-PKcs inhibition, a future direction would involve performing a phosphorylation assay of γ-H2AX and subjecting our results to similar statistical tests that Rouhani did.

Another point of discussion, however, is that while Wortmannin is a high-affinity inhibitor for DNA-PKcs, it can also look to bind to other members of the PI3K family of kinases, such as ATM [11]. Upon collection of experimental data, it would be interesting to see if incorporating ATM inhibition by Wortmannin would make for a more accurate model. We noted that a 20 μM dose of Wortmannin altered DSB repair kinetics such that there was a non-zero number of DSBs remaining after 100 hours (Fig. 4.4). Interestingly, Boulton, *et al.* reported that near-maximum inhibition of DSB repair occurred at a concentration of 20 μM of Wortmannin [1]. Additionally, alternate small

molecule inhibitors of PI3K, however, seem to show promise, such as SF1126 [7] and XL-147 [18] which advanced through Phase I trials.

Ultimately, the combined use of NHEJ inhibition and radiotherapy will hope to increase the chance of DSB repair failure in cancer cells, leading to decreased rates of cancer cell survival [5]. To increase predictive power linking proper radiation dose and cell survival in the context of enzyme inhibition, one could use the McMahon model after incorporating the NHEJ kinetics as described in 5.2 [13]. This integration would add more detail to the high-level approach of McMahon and might provide more accurate result in the prediction for cell survival accounting for enzyme inhibition.

6. Conclusions

In summary, we evaluate here the applicability and accuracy of an eleven-coupled-ODE model for DNA repair by NHEJ towards simulating the kinetics of DSB repair in response to ionizing radiation. Additionally, we expanded upon the original model by considering the effects of competitive, noncompetitive, or uncompetitive enzyme inhibition, specifically on DNA-PKcs and the XXL complex. We found that the most effective types of enzyme inhibition for DNA-PKcs and the XXL complex are non-competitive inhibition and competitive inhibition, respectively. Effective inhibition of the NHEJ pathway in cancer cells through the targeting of these proteins should increase cancer cell destruction rate; hence we anticipate that this knowledge will be advantageous toward enhancing the efficacy of radiotherapy against cancer.

References

[1] S. Boulton, S. Kyle, L. Yalcintepe, and B.W. Durkacz. Wortmannin is a potent inhibitor of DNA double strand break but not single strand break repair in chinese hamster ovary cells. *Carcinogenesis*, 17:2285–2290, 1996.

[2] X. Chen, S. Zhong, X. Zhu, B. Dziegielewska, T. Ellenberger, G.M. Wilson, Jr. A.D. MacKerell, and A.E. Tomkinson. Rational design of human DNA ligase inhibitors that target cellular dna replication and repair. *Cancer Research*, 68(9):3169–3177, 2008.

[3] P.S. Crooke and F.F. Parl. A mathematical model for DNA damage and repair. *Journal of Nucleic Acids*, 2010:1–7, 2010.

[4] A.J. Davis and D.J. Chen. DNA double strand break repair via non-homlogous end-joining. *Translational Cancer Research*.

[5] L. Enns, D. Murray, and R. Mirzayans. Effects of the protein kinase inhibitors wortmannin and KN62 on cellular radiosensitivity and radiation-activated S phase and G1/S checkpoints in normal human fibroblasts. *British Journal of Cancer*, 81:959–965, 1999.

[6] E.C. Friedberg. A history of the DNA repair field. *Cell Research*, 18:3–7, 2007.

[7] J.R. Garlich, P. De, N. Dey, J.D. Su, X. Peng, A. Miller, R. Murali, Y. Lu, G.B. Mills, V. Kundra, H.K. Shu, Q. Peng, and D.L. Durden. A vascular targeted pan phosphoinositide 3-kinase inhibitor prodrug, SF1126, with antitumor and antiangiogenic activity. *Cancer Research*, 68:206–215, 2008.

[8] A.A. Goodarzi, Y. Yu, E. Riballo, P. Doublas, S.A. Walker, R. Ye, C. Harer, C. Marchetti, N. Morrice, PA. Jeggo, and S.P. Lees-Miller. DNA-PK autophosphorylation facilitates artemis endonuclease activity. *The Embo Journal*, 25(16):3880–3889, 2006.

[9] T.R.L. Howes, A. Sallmyr, R. Brooks, G.E. Greco, D.E. Jones, Y. Matsumoto, and A.E. Tomkinson. Structure-activity relationships among DNA ligase inhibitors: Characterization of a selective uncompetitive DNA ligase I inhibitor. *DNA Repair*, 60:29–39, 2018.

[10] M. Ihara, K. Shichijo, S. Takeshita, and title = T. Kudo.

[11] R.A. Izzard, S.P. Jackson, and G.C.M. Smith. Competitive and noncompetitive inhibition of the dna-dependent protein kinase. *Cancer Research*, 59:2581–2586, 1999.

[12] M. Lieber. The mechanism of double-strand DNA break repair by the nonhomologous DNA end-joining pathway. *Annual Review of Biochemistry*, 79:181, 2010.

[13] S.J. McMahon, J. Schuemann, H. Paganetti, and K.M. Prise. Mechanistic modelling of DNA repair and cellular survival following radiation-induced DNA damage. *Scientific Journals*, 6:1–14, 2016.

[14] S. Nazir, N. Jalal, N. Anwar, and S. Haq. Artemis inhibitor: a new approach for radiotherapy. *Journal of Pharmaceutics and Drug Delivery Research*.

[15] C. Poinsignon, R. de Chasseval, S. Soubeyrand, D. Mohous, A. Fischer, R.J. Hache, and J.P. de Villartay. Phosphorylation of artemis following irradiation-induced DNA damage. *European Journal of Immunology*, 34(11):3146–3155, 2004.

[16] E.P. Rogakou, D.R. Pilch, A.H. Orr, V.S. Ivanova, and W.M. Bonner. DNA double-stranded breaks induce histone H2AX phosphorylation on serine 139. *Journal of Biological Chemistry*, 273:5858–5868, 1998.

[17] M. Rouhani. Modeling the interplay between DNA-PK, artemis, and ATM in non-homologous end-joining repair in g1 phase of the cell cycle. *Journal of Biological Physics*, 45(1):127–146, 2019.

[18] G.I. Shapiro, J. Rodon, C. Bedell, E.L. Kwak, J. Baselga, I. Braa, S.S. Pandya, C. Scheffold, A.D. Laird, L.T. Nguyen, Y. Xu, C. Egile, and G. Edelman. Phase I safety, pharmacokinetic, and pharmacodynamics study of SAR245408 (XL147), an oral pan-class I PI3K inhibitor, in patients with advanced solid tumors. *Clinical Cancer Research*, 20:233–245, 2013.

[19] R. Taleei, P.M. Girard, and J. Nikjoo. DSB repair model for mammalian cells in early S and G1 phases of the cell cycle: Application to damage induced by ionizing radiation of different quality. *Mutation Research*, 779:5–14, 2015.

[20] R. Taleei and J. Nikjoo. Biochemical DSB-repair model for mammalian cells in G1 and early S phases of the cell cycle. *Mutation Research*, 756:206–212, 2013.

Appendix A. Table of Dummy Variables

v	Expression	Parameters & Meaning
v_1	$c \times IR\,dose$	c - DSB induction
v_2	$Ku\_DSB\,binding\,rate$	Ku - Ku70/80 complex
	$\times[Ku]^2 \times [DSB]$	DSB - Double-strand break
v_3	$DNA-PKcs\_C1L\,binding\,rate$	$C1L$ - Ligatable complexes of main proteins
	$\times[C1L] \times [DNA-PKcs]^2$	$DNA-PKcs$ - DNA-dep. prot. kinase cat. subunit
v_4	$DNA-PKcs\_C1U\,binding\,rate$	$C1U$ - Unligatable proteins of main proteins
	$\times[C1U] \times [DNA-PKcs]^2$	$DNA-PKcs$ - DNA-dep. prot. kinase cat. subunit
v_5	$\frac{k_{cat}XXLforC1L\times[XXL]\times[C1L]}{K_mXXLforC1L+[C1L]}$	XXL - XLF/XRCC4/ligase IV complex
		$C1L$ - Ligatable complexes of main proteins
v_6	$\frac{k_{cat}XXLforC2L\times[XXL]\times[C2L]}{K_mXXLforC2L+[C2L]}$	XXL - XLF/XRCC4/ligase IV complex
		$C2L$ - Ligatable from $C1L$
v_7	$\frac{k_{cat}ArtemisPP\times[ArtemisPP]\times2\times[C2U]}{K_mArtemisPP+2\times[C2U]}$	$ArtemisPP$ - Hyperphosphorylated form of Artemis
		$C2U$ - Unligatable from $C1U$
v_8	$\frac{k_{cat}ATM\times[ATM]\times[Artemis]}{K_mATM+[Artemis]}$	ATM - Ataxia telangiectasia mutated
		$Artemis$ - Artemis protein
v_9	$\frac{k_{cat}DNA-PKcs\times2\times([C2L]\times[C2U])\times[ArtemisP]}{K_mDNA-PKcs+[ArtemisP]}$	$C2L$ - Ligatable from $C1L$
		$C2U$ - Unligatable from $C1U$
		$ArtemisP$ - Phosphorylated form of Artemis

Appendix B. Replication of Figures Involving Various IR Dosages

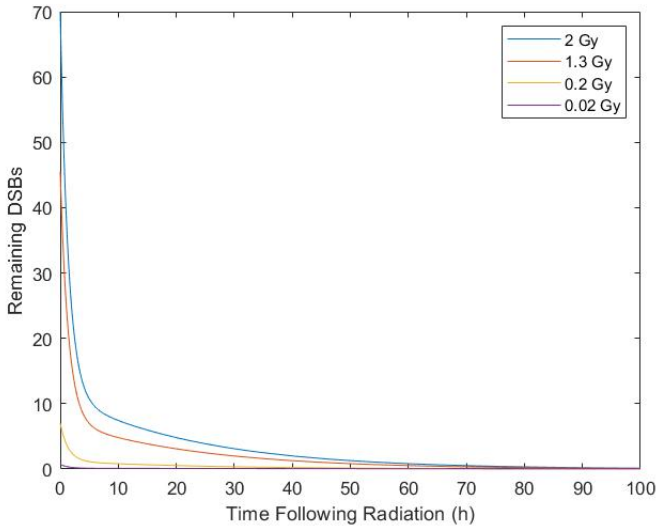

FIGURE B.1. Repair of double-stranded breaks over a period of 100 hours with different amounts of IR dosages

Appendix C. Replication of Figures Involving Zero or One ATM Enzyme(s)

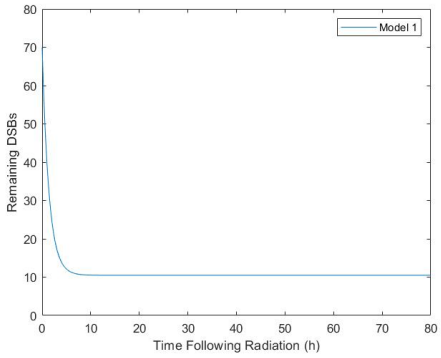

FIGURE C.1. Remaining DSBs over time; 0 ATM & 2 grays of IR dosage.

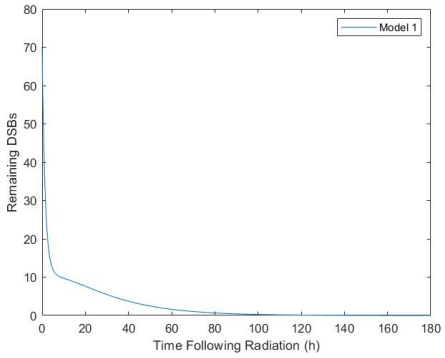

FIGURE C.2. Remaining DSBs over time; 1 ATM & 2 grays of IR dosage.

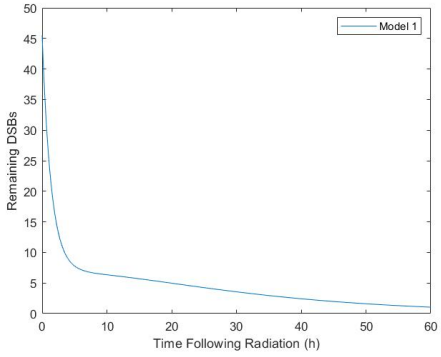

FIGURE C.3. Remaining DSBs over time; 1 ATM & 1.3 grays of IR dosage.

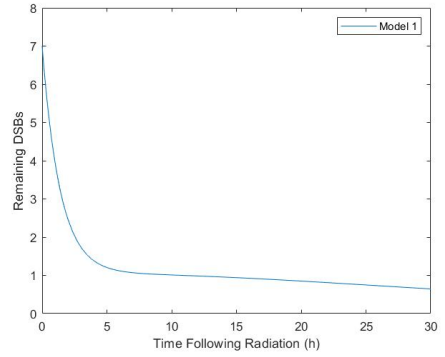

FIGURE C.4. Remaining DSBs over time; 1 ATM & 0.2 grays of IR dosage.

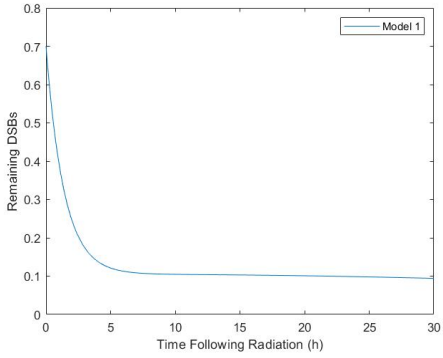

FIGURE C.5. Remaining DSBs over time; 1 ATM & 0.02 grays of IR dosage.

Appendix D. Replication of Figures Involving No Artemis

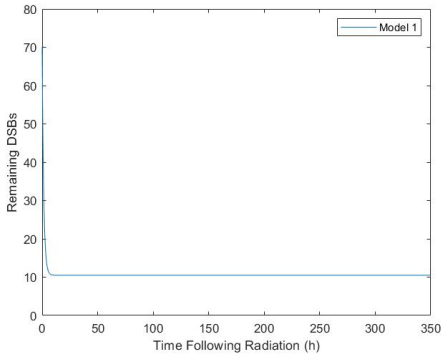

FIGURE D.1. Remaining DSBs over time; 0 Artemis & 2 Grays of IR Dosage.

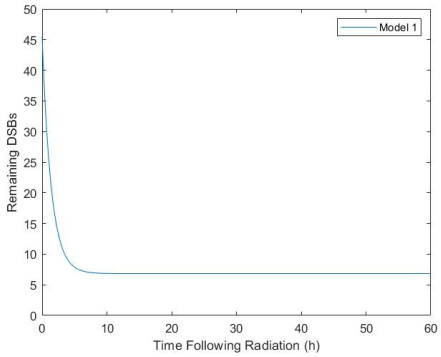

FIGURE D.2. Remaining DSBs over time; 0 Artemis & 1.3 Grays of IR Dosage.

DEPARTMENT OF MATHEMATICS, THE UNIVERSITY OF ARIZONA, TUCSON, AZ 85721, USA
Email address, A. Alamban: aalamban@email.arizona.edu
Email address, S. Fried: sdefried@email.arizona.edu
Email address, J. Lawson: jerlawson13@email.arizona.edu